

Chemical properties of electrospayed antimony tin oxide thin film/Ag nanowire multilayer for transparent conductive electrodes

This content has been downloaded from IOPscience. Please scroll down to see the full text.

2014 Appl. Phys. Express 7 075002

(<http://iopscience.iop.org/1882-0786/7/7/075002>)

View [the table of contents for this issue](#), or go to the [journal homepage](#) for more

Download details:

IP Address: 117.17.187.65

This content was downloaded on 01/08/2014 at 04:14

Please note that [terms and conditions apply](#).

Chemical properties of electrospayed antimony tin oxide thin film/Ag nanowire multilayer for transparent conductive electrodes

Bon-Ryul Koo and Hyo-Jin Ahn*

Department of Materials Science and Engineering, Seoul National University of Science and Technology, Seoul 139-743, Korea
E-mail: hjahn@seoultech.ac.kr

Received May 21, 2014; accepted June 12, 2014; published online June 27, 2014

An antimony tin oxide (ATO) thin film/Ag nanowire (NW) multilayer was fabricated by spin-coating and electrospay deposition. To investigate the optimum thickness of the ATO thin layer deposited on Ag NWs, its deposition time was varied in the range of 0–15 min. The multilayer nanostructure with an ATO thin layer deposited for 3 min exhibited excellent sheet resistance ($\sim 27.9 \Omega/\square$), high optical transmittance ($\sim 81.9\%$), good haze value ($\sim 4.7\%$), excellent thermal stability under microwave annealing at 300°C , and excellent chemical stability for 4 weeks because of the optimized ATO thin layer and excellent electrical conductivity of the Ag NWs. © 2014 The Japan Society of Applied Physics

Transparent conductive electrodes (TCEs) that simultaneously provide low resistivity ($< 10^{-3} \Omega\cdot\text{cm}$) and high transmittance ($> 80\%$) in the visible region are important components for optoelectronic applications such as solar cells, organic light-emitting diodes, and touch screens.^{1–3)} Until now, various TCE materials such as oxide-based materials [e.g., $\text{In}_2\text{O}_3:\text{Sn}$ (ITO), $\text{SnO}_2:\text{F}$ (FTO), $\text{ZnO}:\text{Al}$ (AZO), and $\text{SnO}_2:\text{Sb}$ (ATO)], carbon-based materials (e.g., graphene and carbon nanotubes), and metal-based nanowires (NWs) (e.g., Ag NWs and Cu NWs) have been extensively developed.^{4–6)} Among the above-mentioned materials, Ag NWs have recently been proposed as a promising candidate for TCEs because of their low sheet resistance and low extinction coefficient in the visible range. Furthermore, because the deposition of Ag NWs on the glass substrate can mostly be accomplished using simple solution-based processes, it is simple to fabricate continuous Ag NW networks.^{7,8)} However, Ag NW networks have critical problems regarding thermal and chemical stabilities that restrict their use in real applications. For example, Ag NWs can be easily oxidized and can form discontinuous isolated Ag islands when they are exposed to humid environments and high temperatures ($> 200^\circ\text{C}$), which can cause degradation of electrical and optical properties.⁶⁾ Thus, enhancing the long-term thermal and chemical stabilities of Ag NWs for TCEs is an important goal. To resolve these issues, a protective layer can be introduced. Up until now, synthetic methods for depositing protective layers, such as sputtering, dip-coating, and doctor blading, have been developed.^{9–11)} However, no synthetic method using an electrospay technique has been developed to date. Thus, the optimum conditions for electrospayed ATO thin-film deposition on the Ag NWs are unknown. Here, an electrospay technique is chosen because of its simplicity, good repeatability, large-scale production, and low-cost fabrication.¹²⁾ Furthermore, an ATO TCE is chosen as a protective layer because of its good mechanical durability, abundance, excellent thermal and chemical stabilities, and low cost compared with the commercially used ITO.

Herein, we fabricated ATO thin film/Ag NW multilayers by spin-coating and electrospay deposition. The TCE characteristics of the ATO thin film/Ag NW multilayer, including the thermal properties under microwave annealing at 300°C and the chemical properties when the multilayer is exposed at room temperature for 4 weeks, were measured as a function of electrospay deposition time.

The electrospayed ATO thin film/Ag NW multilayer was fabricated using a combination of spin-coating and electrospay deposition. First, a Ag NW solution was prepared from a mixed solution (1 : 1 v/v) of Ag NW ink (Zhejiang Kechuang Advanced Materials) and 2-propanol [$(\text{CH}_3)_2\text{CHOH}$, Aldrich]. The prepared solution was spin-coated onto the glass substrate at 2000 rpm for 30 s, and then the resultant Ag NW networks were dried in an oven at 80°C for 1 h to remove the residual solvent. After drying, the ATO thin film was deposited onto the Ag NW networks by electrospay deposition. For the electrospay technique, antimony(III) chloride (SbCl_3 , Aldrich) was dissolved in 2-propanol for 1 h, and then tin(II) chloride dihydrate ($\text{SnCl}_2\cdot 2\text{H}_2\text{O}$, Aldrich) was added. The molar ratio of Sn to Sb was adjusted to 10 : 1, as previously reported.¹²⁾ The obtained transparent ATO-sol solution was transferred into a syringe equipped with a 23-gauge stainless-steel needle. The feeding rate of the solution was controlled to 0.03 mL/h, and the voltage applied was 24 kV. The distance between the needle and collector was fixed to ~ 10 cm. Finally, the electrospayed ATO thin film was deposited on the Ag NW network. To investigate the optimum thickness of the ATO thin film, the electrospay deposition time was controlled to 0, 1, 3, 5, 10, or 15 min (referred to hereafter as pure Ag NWs and samples A, B, C, D, and E, respectively). The as-prepared ATO thin film/Ag NW multilayer was dried in an oven at 150°C for 3 h under an argon atmosphere and then microwave-heated at 300°C for 5 min with a heating rate of $20^\circ\text{C}/\text{min}$. The structural and chemical properties of the electrospayed ATO thin film/Ag NW multilayer were characterized by X-ray diffraction (XRD; Rigaku D/Max-2500 diffractometer with Cu $K\alpha$ radiation) and X-ray photoelectron spectroscopy (XPS; ESCALAB 250 equipped with an Al $K\alpha$ X-ray source). The morphological properties were evaluated by field-emission scanning electron microscopy (FE-SEM; Hitachi S-4700) and multifunctional transmission electron microscopy (MULTI/TEM; Tecnai G² Gwangju Center). The sheet resistance for the TCEs was measured using a Hall effect measurement system (Ecopia HMS-3000), and the transmittance in the wavelength range of 280 to 900 nm was examined by UV–vis spectroscopy (Perkin-Elmer Lambda-35).

Figure 1(a) shows the XRD data for the electrospayed ATO thin film/Ag NW multilayers fabricated with different deposition times. Reference bulk reflections of pure Ag and SnO_2 phases are shown at the bottom. For sample A, the

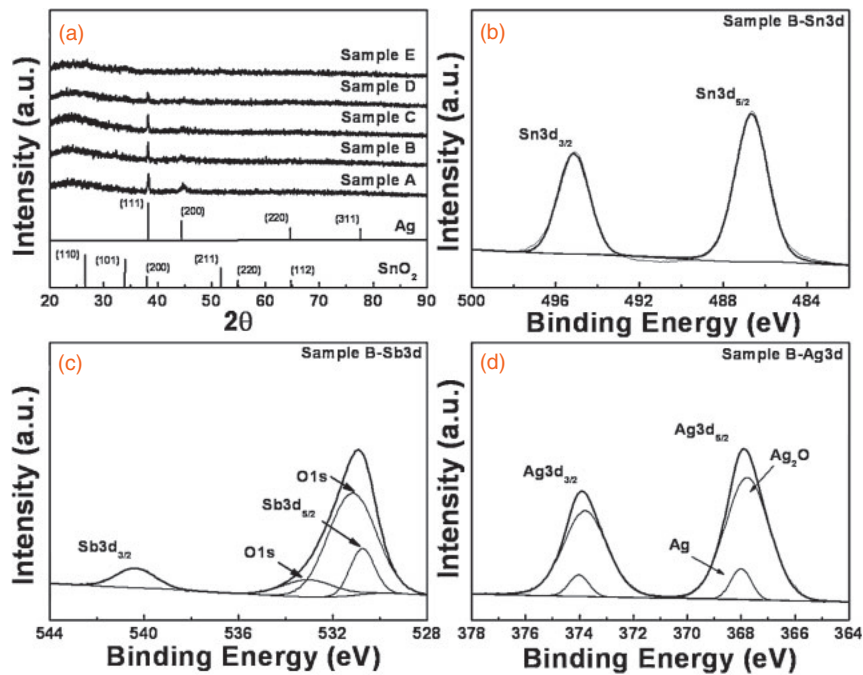


Fig. 1. XRD data of all the samples (a) and XPS core-level spectra for the Sn 3d, Sb 3d, and Ag 3d photoelectrons obtained from sample B.

sharp peaks are observed at 38.2 and 44.4° , corresponding to the (111) and (200) planes of the metallic Ag phase with a face-centered cubic structure (space group $Fm\bar{3}m$ [225]; JCPDS Card No. 87-0720). The intensities for these (111) and (200) peaks of the metallic Ag phase decreased gradually as the electro spray deposition time for ATO thin films increased. Finally, for sample E, the peaks for the Ag phase disappeared completely. This result implies that the electro-sprayed ATO thin film exhibits amorphous characteristics because it is formed at a low annealing temperature of 300°C .^{13,14} Figures 1(b)–1(d) present the XPS core-level spectra of the Sn 3d, Sb 3d, and Ag 3d photoelectrons obtained from sample B. The peaks of the Sn $3d_{5/2}$ and Sn $3d_{3/2}$ photoelectrons are observed at ~ 486.6 and ~ 495.1 eV, indicating that Sn exists in SnO_2 phases. The peaks of Sb $3d_{5/2}$ and Sb $3d_{3/2}$ photoelectrons shown in Fig. 1(c) are observed at ~ 530.7 and ~ 540.3 eV, indicating that Sb forms Sb^{5+} ions in Sb_2O_5 phases. These results indicate the successful formation of Sb-doped SnO_2 (ATO) phases, as reported previously.^{12,15} In addition, two peaks for O 1s photoelectrons appear at ~ 531.6 and ~ 533.0 eV, and are assigned to nonstoichiometric oxides on the surface and oxygen weakly bound to the surface.¹⁶ For the Ag 3d photoelectrons, the two main peaks in XPS spectra [Fig. 1(d)] are at ~ 367.8 eV for Ag $3d_{5/2}$ and ~ 373.8 eV for Ag $3d_{3/2}$, implying that Ag exists as Ag^+ in the Ag_2O phase.¹⁷ Secondary peaks are also observed at ~ 368.0 eV for Ag $3d_{5/2}$ and ~ 374.0 eV for Ag $3d_{3/2}$, corresponding to metallic Ag states.¹⁸ Thus, the XRD and XPS results confirm that the Ag NW networks are composed of metallic Ag cores and partially oxidized Ag surfaces formed during annealing.

Figure 2 shows SEM images of all the samples obtained after microwave heating at 300°C . The pure Ag NW networks contained droplet-shaped Ag particles with diameters of ~ 188 – 219 nm. In general, the Ag NWs coalesce into isolated droplet-shaped Ag particles at temperatures

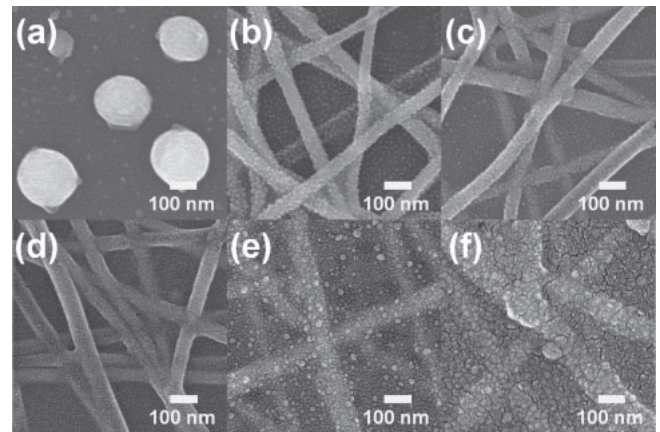


Fig. 2. FESEM data of the pure Ag NWs (a), sample A (b), sample B (c), sample C (d), sample D (e), and sample E (f) obtained after microwave annealing at 300°C .

over 200°C owing to Ag migration.¹⁹ As a result, disconnected Ag NW networks are formed. On the other hand, in samples A–E, ATO thin films have been deposited on Ag NW networks with different deposition times (i.e., 1, 3, 5, 10, or 15 min). The Ag NWs in samples A–E maintain their high-aspect-ratio morphology without any coalescence. As the deposition time increases, the empty space between Ag NW networks is gradually filled by the electro-sprayed ATO thin film. Finally, the empty space between Ag NWs disappeared in samples D–E, as shown in Figs. 2(e)–2(f). Thus, the deposition time can affect the optical and electrical properties of the electro-sprayed ATO thin film/Ag NW multilayer. We discuss the optimum deposition conditions later.

To further examine the morphological characteristics of the electro-sprayed ATO thin film/Ag NW multilayer, TEM measurements were carried out. Figure 3 shows TEM images

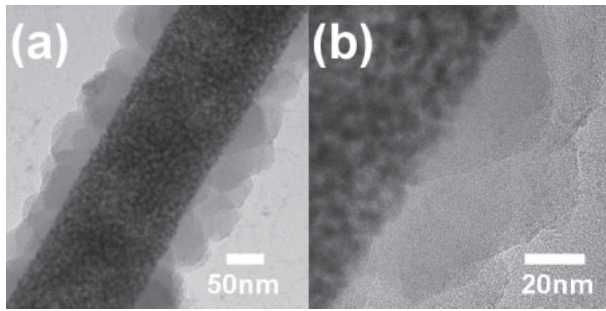


Fig. 3. TEM image (a) and high-resolution TEM image (b) obtained from sample B.

of sample B, in which relatively dark contrast regions represent Ag NWs and the relatively bright contrast regions are the ATO phases. The TEM results clearly show that amorphous ATO phases cover the Ag NWs. The amorphous ATO phases have disordered atomic arrangements and a three-dimensional distribution of grain boundaries, resulting in a lower effective diffusion coefficient compared with crystalline ATO phases.²⁰ Herein, because amorphous ATO phases interrupt the penetration of the Ag phases, the one-dimensional morphology of the Ag NWs remains after annealing at 300 °C.²¹ Thus, the amorphous ATO thin film deposited onto the Ag NWs acts as a protective layer that can improve the thermal and chemical stabilities of the electrospayed ATO thin film/Ag NW multilayer.

Figure 4(a) shows the sheet resistances of samples A–E obtained after microwave heating at 300 °C. The sheet resistance of pure Ag NWs could not be measured because of the formation of isolated droplet-shaped Ag particles, as shown in Fig. 2(a). However, the sheet resistances of samples A–E are ~14.5, ~27.9, ~503.6, ~2,318, and ~4,922 Ω/\square , respectively, as shown in Table I. Note that the sheet resistance gradually increased with the electro spray deposition time of the ATO thin film. In particular, the sheet resistances for samples A and B are predominantly affected by the Ag NWs because of the thinness of the ATO thin films, whereas the sheet resistances for samples D and E are predominantly affected by the thicker amorphous ATO thin layer. Thus, samples D and E exhibit much higher sheet resistances than samples A–C. Among all the samples, samples A and B exhibit excellent sheet resistance. Figure 4(b) shows the optical transmittances of all the samples. At 550 nm, the optical transmittances are observed to be ~75.8, ~82.6, ~81.9, ~80.8, ~79.1, and ~75.3% for pure Ag NWs and samples A–E, respectively. Pure Ag NWs exhibit low transmittance owing to light scattering by the widely distributed Ag particles on the thin film.²² Furthermore, the transmittance decreases gradually from samples A to E because of the increasing thickness of the ATO thin layer.¹³ Figure 4(c) presents the haze measurements showing the light scattering capability of all the samples. In general, because Ag NW networks with large-diameter nanowires (>50 nm) cause light scattering in the visible region, they possess high haze values in the range of 5–10%,²³ which are unsuitable for applications such as touch panels and LCDs. Thus, decreasing the haze value for TCEs can be important for industrialization. The haze value is defined as the fraction of diffusively transmitted light to the total transmitted light.²⁴

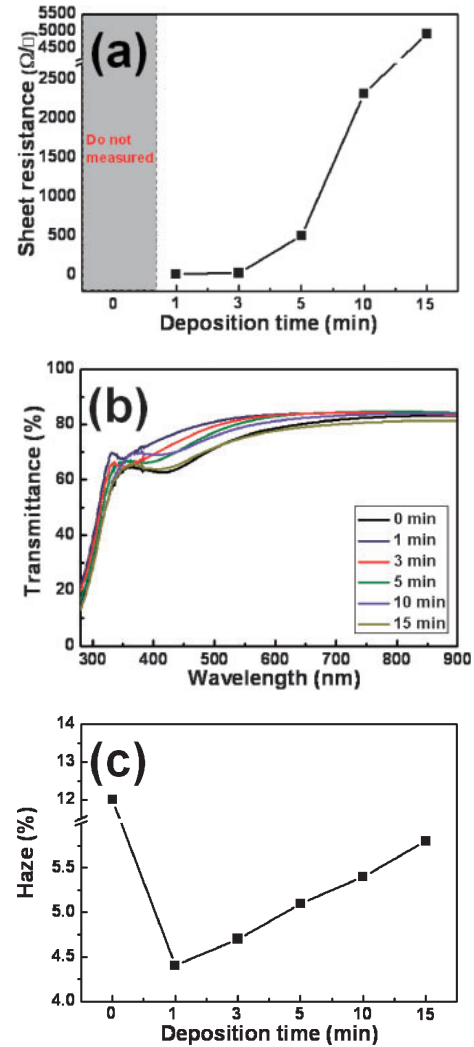


Fig. 4. Sheet resistance (a), optical transmittance (b), and haze value (c) obtained from all the samples.

Table I. Summary of electrical and optical properties of all the samples obtained after microwave annealing at 300 °C.

Samples	Sheet resistance (Ω/\square)	Transmittance (%)	Haze (%)
Pure Ag NWs	—	75.8	12
Sample A	14.5	82.6	4.4
Sample B	27.9	81.9	4.7
Sample C	503.6	80.8	5.1
Sample D	2,318	79.1	5.4
Sample E	4,922	75.3	5.8

$$H_T = \frac{T_{\text{tot}} - T_{\text{direct}}}{T_{\text{tot}}} \times 100\%,$$

where T_{tot} is the total transmittance and T_{direct} is the direct transmittance. The haze values are measured to be ~12, ~4.4, ~4.7, ~5.1, ~5.4, and ~5.8% for pure Ag NWs and samples A–E, respectively. That is, pure Ag NWs exhibit a high haze value because of the enhanced light scattering by the Ag particle aggregates formed after annealing.²⁵ The haze values of samples A–E are lower than that of pure Ag NWs, indicating that the ATO thin layer reduces the amount

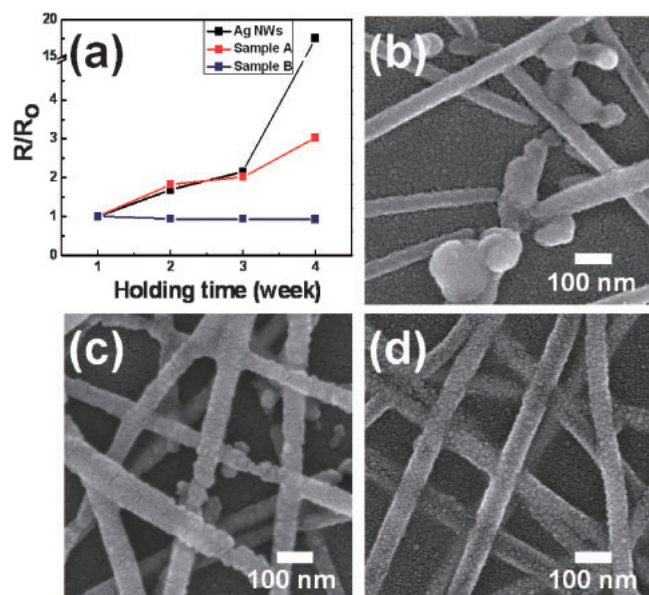


Fig. 5. Changes in sheet resistance of the pure Ag NWs, sample A, and sample B exposed to air at room temperature for 4 weeks to investigate the chemical stability of the samples (a). FESEM images of the pure Ag NWs, sample A, and sample B measured after 4 weeks.

of light scattering by preserving the high-aspect-ratio morphology of the Ag NWs and preventing the aggregation of the Ag phases.

To investigate the chemical stability of the samples, pure Ag NWs, sample A, and sample B were exposed to air at room temperature for 4 weeks. Figure 5(a) shows the changes in sheet resistance of the samples over 4 weeks, as an indication of their chemical stability. The sheet resistances for the Ag NWs and sample A increased 17.5 and 3.0 times, respectively, after 4 weeks. This is because Ag NWs exposed to air atmosphere for 4 weeks are easily oxidized and also partially form agglomerates of Ag particles, resulting in the increased junction resistance of the Ag NWs.²⁶⁾ Similarly, agglomerates of Ag particles also form in sample A because the electrospayed ATO film is very thin. However, the sheet resistance of sample B remains the same after 4 weeks, as shown in Fig. 5(a). Thus, the electrospayed ATO thin layer can act as a protective layer to maintain the sheet resistance for sample B because of its optimum thickness. In summary, sample B exhibited excellent sheet resistance ($\sim 27.9 \Omega/\square$), good transmittance ($\sim 81.9\%$), good haze value ($\sim 4.7\%$), and excellent thermal and chemical stabilities as reflected by the retained sheet resistance after 4 weeks of exposure to air.

In conclusion, electrospayed ATO thin film/Ag NW multilayers were fabricated by spin-coating and electrospay deposition with different deposition times. Compared with pure Ag NW networks, the multilayer nanostructure containing the optimized electrospayed ATO thin film grown for 3 min exhibited not only excellent TCE properties, including a sheet resistance of $\sim 27.9 \Omega/\square$, a transmittance of $\sim 81.9\%$,

and a haze value of $\sim 4.7\%$, but also excellent thermal stability after microwave annealing at 300°C and chemical stability when exposed to air at room temperature for 4 weeks. This improvement in performance can be explained by the synergy between the optimum thickness of the electrospayed ATO thin layer and the excellent electrical conductivity of the Ag NWs. The electrospayed ATO thin film/Ag NW multilayer can be used as an alternative TCE for applications requiring thermal and chemical stabilities, such as touch panels, solar cells, and optical light-emitting diodes (OLEDs).

Acknowledgments This work was supported by Grant No. 10041161 from the Ministry of Knowledge Economy (MKE) and the Fundamental R&D Program for Core Technology of Materials funded by the Ministry of Knowledge Economy, Republic of Korea.

- 1) A. Hongsingthong, T. Krajangsang, I. A. Yunaz, S. Miyajima, and M. Konagai, *Appl. Phys. Express* **3**, 051102 (2010).
- 2) N. B. Choi, K. Y. Lee, M. S. Yang, and C. D. Kim, *Jpn. J. Appl. Phys.* **43**, 5516 (2004).
- 3) A. R. Madaria, A. Kumar, and C. Zhou, *Nanotechnology* **22**, 245201 (2011).
- 4) H. Han, D. Adams, J. W. Mayer, and T. L. Alford, *J. Appl. Phys.* **98**, 083705 (2005).
- 5) T. L. Chen, D. S. Ghosh, N. Formica, and V. Pruneri, *Nanotechnology* **23**, 395603 (2012).
- 6) J. Y. Lee, S. T. Connor, Y. Cui, and P. Peumans, *Nano Lett.* **8**, 689 (2008).
- 7) D. S. Leem, A. Edwards, M. Faist, J. Nelson, D. D. C. Bradley, and J. C. de Mello, *Adv. Mater.* **23**, 4371 (2011).
- 8) Y. C. Lu and K. S. Chou, *Nanotechnology* **21**, 215707 (2010).
- 9) K. H. Choi, J. Kim, Y. J. Noh, S. I. Na, and H. K. Kim, *Sol. Energy Mater. Sol. Cells* **110**, 147 (2013).
- 10) Y. Ahn, Y. Jeong, and Y. Lee, *ACS Appl. Mater. Interfaces* **4**, 6410 (2012).
- 11) T. Stubhan, J. Krantz, N. Li, F. Guo, I. Litzov, M. Steidl, M. Richter, G. J. Matt, and C. J. Brabec, *Sol. Energy Mater. Sol. Cells* **107**, 248 (2012).
- 12) B. R. Koo and H. J. Ahn, *Ceram. Int.* **40**, 4375 (2014).
- 13) T. R. Giraldo, M. T. Escote, M. I. B. Bernardi, V. Bouquet, E. R. Leite, E. Longo, and J. A. Varela, *J. Electroceram.* **13**, 159 (2004).
- 14) K. S. Kim, S. Y. Yoon, W. J. Lee, and K. H. Kim, *Surf. Coatings Technol.* **138**, 229 (2001).
- 15) S. Sharma, A. M. Volosin, D. Schmitt, and D.-K. Seo, *J. Mater. Chem. A* **1**, 699 (2013).
- 16) F. M. Amanullah, K. J. Pratap, and V. Hari Babu, *Mater. Sci. Eng. B* **52**, 93 (1998).
- 17) J. B. Lee, S. Y. Jeong, W. J. Moon, T. Y. Seong, and H. J. Ahn, *J. Alloys Compd.* **509**, 4336 (2011).
- 18) X. Y. Gao, S. Y. Wang, J. Li, Y. X. Zheng, R. J. Zhang, P. Zhou, Y. M. Yang, and L. Y. Chen, *Thin Solid Films* **455–456**, 438 (2004).
- 19) A. Kim, Y. Won, K. Woo, C. H. Kim, and J. Moon, *ACS Nano* **7**, 1081 (2013).
- 20) O. Nakagawara, Y. Kishimoto, H. Seto, Y. Koshido, Y. Yoshino, and T. Makino, *Appl. Phys. Lett.* **89**, 091904 (2006).
- 21) S. Yu, W. Zhang, L. Li, D. Xu, H. Dong, and Y. Jin, *Acta Mater.* **61**, 5429 (2013).
- 22) S. H. Cho and W. J. Lee, *Jpn. J. Appl. Phys.* **49**, 111102 (2010).
- 23) A. B. V. Kiran Kumar, C. W. Bae, L. Piao, and S. H. Kim, *Mater. Res. Bull.* **48**, 2944 (2013).
- 24) C.-H. Tsai, S.-Y. Hsu, T.-W. Huang, Y.-T. Tsai, Y.-F. Chen, Y. H. Jhang, L. Hsieh, C.-C. Wu, Y.-S. Chen, C.-W. Chen, and C.-C. Li, *Org. Electron.* **12**, 2003 (2011).
- 25) S. Sánchez-Valdes, H. Ortega-Ortiz, L. F. Ramos-de Valle, F. J. Medellín-Rodríguez, and R. Guedea-Miranda, *J. Appl. Polym. Sci.* **111**, 953 (2009).
- 26) D. Lee, H. Lee, Y. Ahn, Y. Jeong, D. Y. Lee, and Y. Lee, *Nanoscale* **5**, 7750 (2013).